

Electronic Supplementary Information (ESI)

In-situ observation of facet-dependent oxidation of graphene on platinum in an environmental TEM

Wentao Yuan,^{‡a} Ying Jiang,^{‡a} Yong Wang,^{*a} Shyam Kattel,^b Zhengfei Zhang,^a Lien-Yang Chou,^c Chia-Kuang Tsung,^c Xiao Wei,^a Jixue Li,^a Xiaofeng Zhang,^d Guofeng Wang,^{*b} Scott X. Mao^b and Ze Zhang^a

^aCenter of Electron Microscopy and State Key Laboratory of Silicon Materials, Department of Materials Science and Engineering, Zhejiang University, Hangzhou 310027, China. E-mail: yongwang@zju.edu.cn.

^b Department of Mechanical Engineering and Materials Science, University of Pittsburgh, Pittsburgh, PA 15261, USA. E-mail: guw8@pitt.edu.

^c Department of Chemistry, Boston College, Chestnut Hill, MA 02467, USA.

^dHitachi High Technologies America, Pleasanton, CA 94588, USA.

[‡]These authors contributed equally.

Contents of Supplementary Information:

Materials and methods

Supplementary Text

Figs. S1-S4

References

Movies S1-S5

I. Materials and Methods:

A. Preparation of Pt nanocrystals

Platinum nanocrystals with an average diameter of 6 nm were synthesized using a previously published procedure¹. In a typical preparation, a combination of 0.05 mmol of Pt ions $(\text{NH}_4)_2\text{Pt}(\text{IV})\text{Cl}_6$, 0.75 mmol of tetramethyl ammonium bromide, and 1.00 mmol of polyvinylpyrrolidone (with a molecule weight of 29,000) were dissolved into 10 mL of ethylene glycol in a 25 mL round-bottom flask at room temperature. The mixed solution was then heated to 180 °C and held for 20 min under argon protection and magnetic stirring. After being cooled to room temperature, the solution was separated by centrifugation, washed several times by precipitation/dissolution, and finally re-dispersed in ethanol. The solution, which had a concentration of 1 mg/ml, was then drop-casted on a holey Mo grid for *in-situ* TEM experiments.

B. *In-situ* observation

The *in-situ* observation of the facet-dependent oxidation of graphene layers catalyzed by Pt nanocrystals was carried out in an environmental transmission electron microscope (ETEM) with oxygen injection available (Hitachi H-9500). The Pt nanocrystals in ethanol solution were dispersed on a Mo micro-grid and loaded onto the stage in a TEM heating holder. *In-situ* observation in ETEM was conducted at 300 kV with an oxygen pressure of 5.00×10^{-2} Pa at 500 °C. An AMT digital camera was used for the *in-situ* recording of the Pt-catalyzed graphene-layer oxidation.

II. Supplementary Text:

A. Details about facet-dependent oxidation

The facet-dependent oxidation of graphene shows a good reproducibility and more examples are shown in Figs. S2 and S3. These experimental data yield a consistent result that the velocity of the Pt-catalyzed graphene oxidation is faster on {100} and {110} facets than that on {111} facets, as shown in Table 1, which indicates that Pt{100} and Pt{110} facets show superior catalytic activity in the graphene oxidation, compared with Pt{111} facets.

As the line velocity neglected the longitudinal length of the facets along the viewing direction and might not reflect the real situation, we need to take the area of facets into consideration to obtain a surface velocity of oxidation. Although we are unable to accurately obtain the 3D atomic structure of the Pt nanoparticles, we can alternatively estimate the area of each facet through a simplified model. Since the Pt nanoparticles in our experiments are mainly exposed by {100}, {110} and {111} facets, we build a model that only contains these three typical facets (as shown in Fig. S4a), by using WinXMorph crystal morphology builder.² In the ideal model, we note that the equivalent facets have the same area and the shapes of {100}, {110} and {111} facets are usually octagons, rectangles and hexagons (Fig. S4b), respectively. It should be mentioned that the facet's shapes would change particle by particle and typical possible shapes of {100}, {110} and {111} facets are displayed in Fig. S4c at a given projected line lengths (marked by l_1 , l_2 and l_3). That is to say, when the model changes from the left to the right in Fig. S4a, the shapes of these facets alter accordingly from the left to the right in Fig. S4c. Based on the experimental data in Fig. 2 and Fig. S3, we modified the model to Fig. S4b where the (111) and (-111) facets have different line lengths

(note that the (111) and (-111) facets have the same possible shapes as shown in Fig. S4c). This modified model is indeed well consistent with the experimental image (the particle in Fig. 2) in Fig. S4d. We should clarify that the outlines of the Pt nanocrystals marked {100}, {111} etc. in the Figs. 2, 3, S2 and S3 should represent 2-dimensional facets rather than the edges. Because in our models from our viewing axes, the angles between the two specific facets are the constants, and these values are consistent with our experimental data. Additionally, the sharp contrasts in the figures also suggest that the outlines are indeed facets. Based on this model and the oxidation time obtained from Fig. 2 (sample #1), we calculate the surface velocity via a formulation of $\text{velocity} = \text{facet area} / \text{oxidation time}$. By calculation, we obtained that the oxidation rate on the (100) facet is larger than $0.075 \text{ nm}^2/\text{s}$; the oxidation rate on the (110) facet is larger than $0.094 \text{ nm}^2/\text{s}$; the oxidation rate on the (111) facet is less than $0.067 \text{ nm}^2/\text{s}$ and the oxidation rate on the (-111) facet is less than $0.052 \text{ nm}^2/\text{s}$, as marked in Fig. S4c. It is obvious that the maximum rate on {111} surfaces is less than that on the (100) and (110) surfaces, which indicates that the oxidation reaction of graphene on Pt{100} and {110} facets are indeed faster than that on {111} facets. Similarly, we calculate the oxidation rates of the sample in Fig. S3 (sample #3), which produces a consistent result that the oxidation rate on (100) facet is larger than $0.124 \text{ nm}^2/\text{s}$; the oxidation rate on (110) facet is larger than $0.126 \text{ nm}^2/\text{s}$; the oxidation rate on (111) facet is less than $0.044 \text{ nm}^2/\text{s}$ and the oxidation rate on (-111) facet is less than $0.040 \text{ nm}^2/\text{s}$.

For Pt{100} and {110} facets, the experimental data in Table 1 show that Pt{100} surfaces have a better catalytic performance than Pt{110} surfaces. However, from the simple model, it is rather difficult to compare these two facets since the calculation only

produce their minima. Nevertheless, the 3D model shows the same result that Pt{100} and Pt{110} facets are more active than Pt{111} facets for the oxidation of graphene layers.

Table S1. The surface velocities of the oxidation of the graphene layers on different facets.

	Sample #1	Sample #3
(100)	> 0.075	> 0.124
velocity		
(110)/(011)	> 0.094	> 0.126
(nm²/s)		
(111)/(-111)	< 0.067 / < 0.052	< 0.044 / < 0.040

We should admit that the actual situation is more complicated than that we discussed above. It is rather difficult to know the exact shapes and sizes of the crystal facets at the atomic scale to acquire an exact surface velocity on different facets. Nevertheless, the data from both the experiments and the simple model consistently suggest that the graphene oxidation rate is faster on Pt{100} and {110} facets than that on {111} facets. The experimental data also suggest that Pt{100} surfaces show a better catalytic activity. To further clarify these issues, the DFT calculation was carried out and the details are described in below.

B. Computational Details

All the calculations were performed within the framework of density functional theory (DFT)^{3,4} as implemented in Vienna Ab-initio Simulation Package (VASP) code.^{5,6} The electronic exchange and correlation effects were described within the generalized gradient approximation (GGA) using PW91 functionals.⁷ All the calculations were performed in spin

unrestricted manner using ultra soft pseudopotentials.⁸ A plane wave basis set with a kinetic energy cut off of 400 eV was used for geometry optimization. Ionic positions were optimized until Hellman–Feynman force on each ion was less than 0.02 eV/Å.

Pt{111}, Pt{100} and Pt{110} surfaces were modeled with 2×2 periodic supercells which contain four atomic layers and four Pt atoms at each layer. The positions of atoms in the top two surface layers were allowed to relax while the positions of atoms in the bottom two layers of Pt{111}, Pt{100} and Pt{110} surfaces were kept fixed during geometry optimization. The artificial interactions between the slabs and their periodic images were avoided by introducing a large vacuum layer of ~12 Å thickness in a direction perpendicular to the slabs. The Brillouin zone integration on the Pt{111}, Pt{100} and Pt{110} surfaces was performed using a 5×5×1 Monkhorst-pack k point mesh,⁹ respectively.

The graphene sheet in our calculations was modeled as a periodically repeating supercell containing 32 carbon (C) atoms. The artificial interactions between the graphene sheet and their periodic images were avoided by introducing a large vacuum layer of ~14 Å thickness in a direction perpendicular to the graphene sheet. All atoms in the graphene supercell were allowed to relax during geometry optimization. The Brillouinzone was sampled on regular 4 × 4 × 1 Monkhorst–Pack grids.⁹

The adsorption/binding energy of adsorbates on the Pt surfaces and graphene sheet was calculated as:

$$BE(\text{adsorbate}) = E(\text{slab/sheet} + \text{adsorbate}) - [E(\text{slab/sheet}) + E(\text{adsorbate})]$$

where $E(\text{slab/sheet} + \text{adsorbate})$ is the total energy of adsorbate adsorbed slab/sheet configuration, $E(\text{slab/sheet})$ is the total energy of clean slab/sheet and $E(\text{adsorbate})$ is the total

energy of an isolated adsorbate optimized in $12 \text{ \AA} \times 13 \text{ \AA} \times 14 \text{ \AA}$ orthorhombic supercell. Here, negative binding energy indicates energetically favorable/stable adsorption unless noted otherwise. Transition states were located using a climbing image nudged elastic band (CI-NEB) method¹⁰ in which the forces perpendicular to the tangent of the reaction pathway were relaxed to less than 0.05 eV/\AA . The activation energy (E_a) is defined as the difference in energy between the transition state and the initial state of a chemical reaction.

C. Effect of the electron beam during the *in situ* observation

In this study, we conducted two comparison experiments for the graphene oxidation on Pt catalysts. In experiment 1, we turned on electron beam irradiation but did not introduce oxygen gas into the ETEM at $500 \text{ }^\circ\text{C}$; in experiment 2, we turned off electron beam irradiation and introduced oxygen gas into the ETEM at $500 \text{ }^\circ\text{C}$. In neither of these two comparison experiments did we observe the oxidation process of the graphene layers. Hence, we concluded that the possible defect generation caused by electron beam irradiation was not responsible for our observed disappearance of the graphene layers on Pt catalysts. The second experiment also implies that the dissociated oxygen atoms may bind the surface tightly, as a consequence, no oxidation of graphene was observed. However, with the assistance of high energy electron beam irradiation, the dissociated oxygen atoms would be easily desorbed from the surface and initiate the oxidation of graphene layers given the fact that the sputtering effect of the high energy electron beam may greatly facilitate this desorption process¹¹. The electron beam may also enhance the reaction by other three ways: 1. The electron beam will cause the thermal vibration of the C atoms in graphene layers,^{11,12} improving the reactivity of

the whole graphene layers; 2. The electron beam can cause the displacement of the C atoms and thus the C adatoms are produced on the graphene layers.^{13,14} These free standing C adatoms favorably react with the O atoms. 3. The electron beam induced breakage of the C-C covalent bonds may also contribute to the stimulation of the reaction.^{12,15} Although some oxygen-containing intermediate products of the oxidation may be reduced by the electron beam irradiation during the oxidation processes,¹¹ this reduction effect is negligible compared to the enhancement effect, which is also testified by our experiments. Nevertheless, all of these effects imposed by the electron beam irradiation are equal to the all C atoms in graphene layers and will not result in different oxidation behaviors on different Pt surfaces.

D. The oxidation pathway

Basically, oxygen molecules first contact with the Pt surface through the defects of graphene layers formed in the sharp ridges between two facets. Then the adsorbed oxygen is dissociated into two O atoms on the Pt surface, initiating the graphene oxidation in the ridges. After the rupture of the graphene layers, the oxygen reaches the Pt surface mainly through the spacious opening in the graphene layers. As for the oxidation pathway, there are two possibilities: one is surface oxidation and the other is edge (or defect) oxidation. Obviously, the surface oxidation dominates at the initial stage as there is no edge available at that time. The oxidation procedure is calculated by density function theory. Our DFT calculations show that the O atoms generated on the Pt surface are extremely reactive with the carbon atoms of the graphene layers. So these intermediate O atoms adsorb on the carbon atoms of the graphene and form the O-C-O groups, followed by the breaking of the C-C bonds and leaving

the C₅O hexagon defects in the graphene basal plane. After the O-C-O groups re-orientated, 2O atoms are solely bound to a single C atom and the CO₂ molecules release by desorption from the graphene layers.

When an edge is formed, oxygen atoms may also react with the edge carbon atoms and proceed the oxidation of graphene. In our experiments, we believe both of the two oxidation types exist and it is rather difficult to strictly distinguish them at this stage. Nevertheless, we demonstrated the reasonable oxidation procedure by calculating the surface oxidation case with DFT.

E. The effect of the other species during the oxidation

Actually, during the oxidation process, some other background species may also exist in our ETEM column, especially for the water and hydrogen molecules. For the water molecules, we suppose that it may also oxidize the graphene layers.¹⁶ However, it should be noted that our oxidation experiments were performed in a pure oxygen environment at 500 °C. Normally, we first held the sample at 500 °C for 10 minutes and then introduced oxygen to the chamber. Before introducing oxygen, we never observed the obvious oxidation by the possible background species, even under irradiation of the electron beam. However, in a high humidity environment, the story may be different.¹⁶

III. Figs. S1-S4:

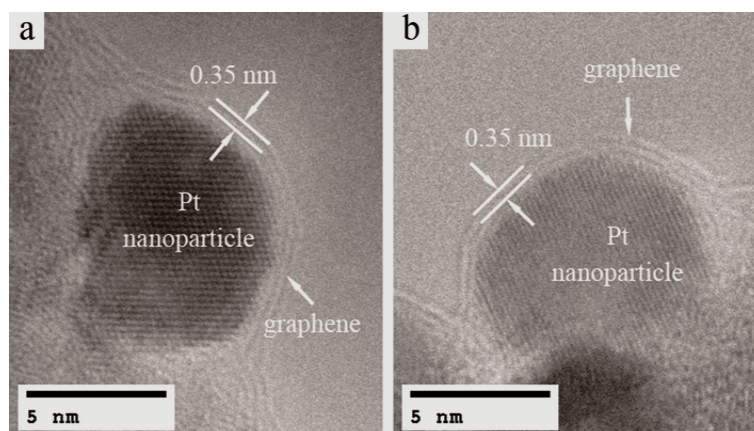


Fig. S1 Typical TEM images of Pt nanocrystals wrapped around by graphene layers. (a,b) The carbon-layer encapsulated Pt nanocrystals were fabricated by the electron beam irradiation on the Pt nanocrystals with a carbon source. The distance of the carbon layer corresponds well to the thickness of graphene layer (0.35 nm), indicating that the fabricated carbon layers are indeed graphene layers.

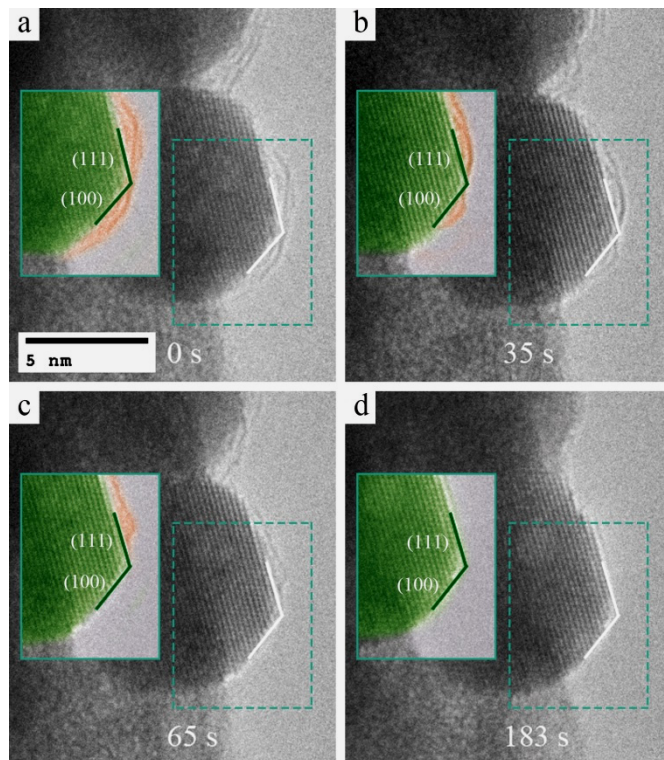


Fig. S2 (Sample #4) TEM images showing the oxidation of graphene layers catalyzed by a Pt nanocrystal with {100 and {111} surfaces. (a-d) are series of TEM images from Movie S5, 0 s (a), 35 s (b), 65 s (c), 183 s (d). Here, 0s corresponds to 70 s in Movie S5.

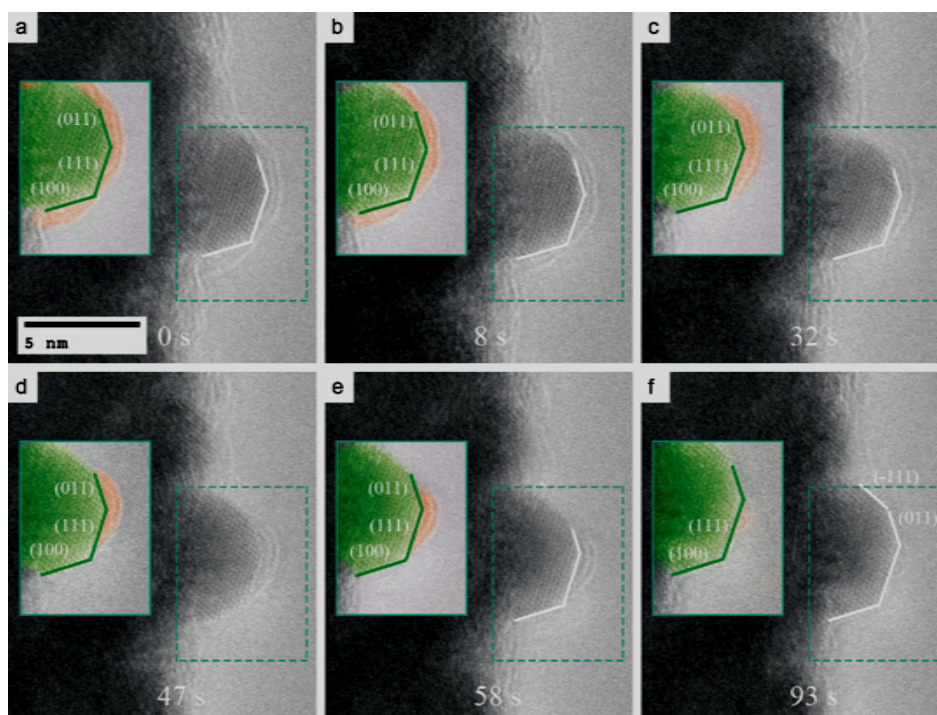


Fig. S3 (Sample #3) TEM images showing the oxidation of graphene layers catalyzed by a Pt nanocrystal with $\{100\}$ and $\{111\}$ surfaces. (a-f) are series of TEM images from Movie S4, 0 s (a), 8 s (b), 32 s (c), 47 s (d), 58 s (e), 93 s (f). Here, 0s corresponds to 41 s in the Movie S4.

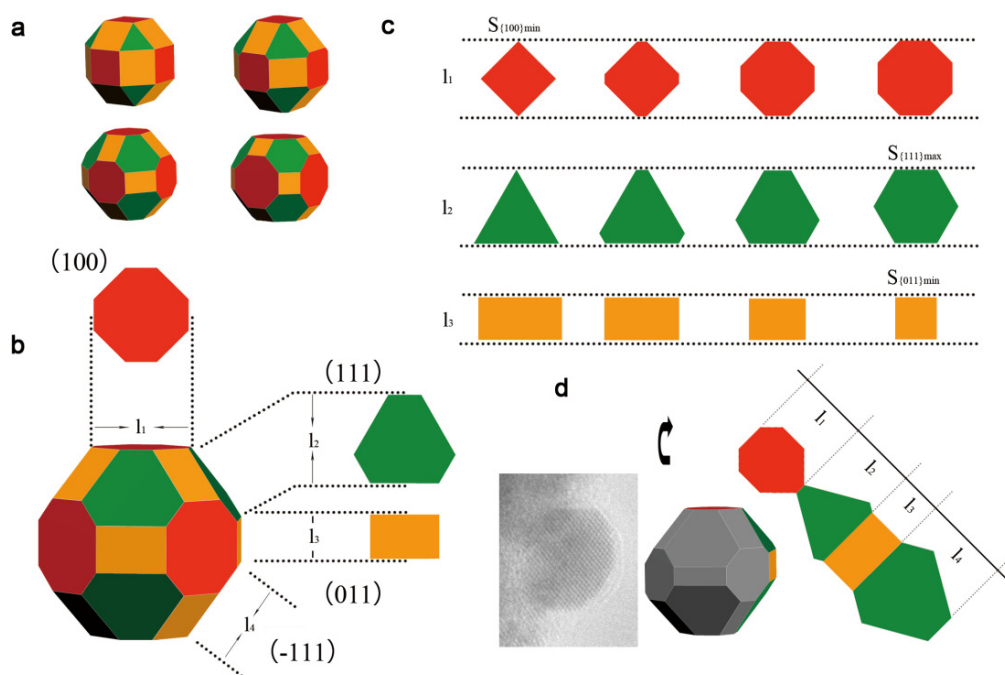


Fig. S4 Simplified 3D structural models of the Pt nanocrystals exposed by $\{100\}$, $\{110\}$ and $\{111\}$ facets, according to our experiments. (a) Typical morphologies of Pt nanocrystals consist of $\{100\}$, $\{110\}$ and $\{111\}$ facets. (b) The model of Pt nanocrystal observed along $[01-1]$ direction. (c) The possible shapes of $\{100\}$, $\{110\}$ and $\{111\}$ facets. (d) The TEM image of the Pt nanocrystal in Fig. 2 and the modified model. The right shows the unfolded planes of the colored part in the model.

IV. References:

- 1 C.-K. Tsung, J. N. Kuhn, W. Huang, C. Aliaga, L.-I. Hung, G. A. Somorjai and P. Yang, *Journal Of the American Chemical Society*, 2009, **131**, 5816.
- 2 W. Kaminsky, *Journal of Applied Crystallography*, 2005, **38**, 566.
- 3 W. Kohn and L. J. Sham, *Physical Review*, 1965, **140**, 1133;
- 4 P. Hohenberg and W. Kohn, *Physical Review B*, 1964, **136**, B864.
- 5 G. Kresse and J. Furthmuller, *Computational Materials Science*, 1996, **6**, 15;
- 6 G. Kresse and J. Hafner, *Physical Review B*, 1993, **48**, 13115.
- 7 J. P. Perdew and Y. Wang, *Physical Review B*, 1992, **45**, 13244.
- 8 G. Kresse and D. Joubert, *Physical Review B*, 1999, **59**, 1758.
- 9 H. J. Monkhorst and J. D. Pack, *Physical Review B*, 1976, **13**, 5188.
- 10 G. Henkelman, B. P. Uberuaga and H. Jonsson, *Journal Of Chemical Physics*, 2000, **113**, 9901.
- 11 R. F. Egerton, P. Li and M. Malac, *Micron*, 2004, **35**, 399;
- 12 R. F. Egerton, *Ultramicroscopy*, 2013, **127**, 100.
- 13 C. P. Ewels, M. I. Heggie and P. R. Briddon, *Chemical Physics Letters*, 2002, **351**, 178;
- 14 O. V. Yazyev, I. Tavernelli, U. Rothlisberger and L. Helm, *Physical Review B*, 2007, **75**.
- 15 F. Banhart, *Reports on Progress In Physics*, 1999, **62**, 1181.
- 16 T. Yaguchi, T. Kanemura, T. Shimizu, D. Imamura, A. Watabe and T. Kamino, *J. Electron Microsc.*, 2012, **61**, 199.

V. Caption for Movie:

Movie S1.The formation of the graphene layers coated on the Pt nanoparticle.

Movie S2.Sample #1 of the in-situ oxidation of graphene on different Pt facets.

Movie S3. Sample #2 of the in-situ oxidation of graphene on different Pt facets.

Movie S4. Sample #3 of the in-situ oxidation of graphene on different Pt facets.

Movie S5. Sample #4 of the in-situ oxidation of graphene on different Pt facets